IEEE Access
Multidisciplinary | Rapid Review | Open Access Journal

Received September 18, 2019, accepted September 29, 2019, date of publication October 10, 2019,
date of current version October 22, 2019.

Digital Object Identifier 10.1109/ACCESS.2019.2946099

Correlation Between Power Line Harmonic Radiation and Magnetospheric Line Radiation Over China

QIANG GUO[1], (Member, IEEE), JING WU[1], (Member, IEEE), CHAO YUE[2], AND LI XIE[3]
[1]Department of Electrical Engineering, Beihang University, Beijing 100191, China
[2]Department of Atmospheric and Oceanic Sciences, University of California at Los Angeles, Los Angeles, CA 90095, USA
[3]China Electric Power Research Institute, Beijing 100192, China

Corresponding author: Jing Wu (wujing06@buaa.edu.cn)

This work was supported by the National Natural Science Foundation of China under Grant 51777006.

ABSTRACT Power line harmonic radiation (PLHR) and magnetospheric line radiation (MLR) are recognized as electromagnetic pollutants in the near-earth space, and their correlation has been a controversial issue. An identification procedure based on short-time discrete Fourier transform and Welch power spectrum estimation was applied to detect 114 PLHR events and 328 MLR events that occurred as DEMETER satellite flew over China from 2008 to 2010. PLHR events feature parallel horizontal lines with a frequency interval of 50/100 Hz in spectrogram, whereas MLR events feature multi-parallel spectral lines with frequency drift as a baseline for possible triggered emissions as well as triggered emissions with no baseline. We statistically compared the temporal and geographical distribution, Kp and Dst indices, and propagation characteristics between PLHR and MLR events. PLHR events showed more obvious variations annually than MLR events, and the former had a close relationship with the development of Chinese power system. Both PLHR and MLR presented similar diurnal and seasonal differences, owing likely to the ionospheric state; moreover, they appeared to have no significant connection with geomagnetic activity level. The geographical distributions of PLHR and MLR differed significantly. PLHR events occurred in the range of (20° N–45° N), whereas MLR events were concentrated in southwestern low-latitude regions of (18° N–28°N). Furthermore, PLHR waves were right-hand circularly polarized, whereas MLR waves were approximately linearly polarized. In summary, MLR is more likely caused by natural radiation that is not directly related to PLHR, whereas PLHR is closely related to terrestrial power systems.

INDEX TERMS Comparison, magnetospheric line radiation, power line harmonic radiation, power system, statistical analysis.

I. INTRODUCTION

China has developed an ultra-high-voltage (UHV) power system characterized by an alternating current (AC) grid of 1000 kV and a direct current (DC) grid of ±800 kV. Its power consumption ranks first in the world [1]. Several new environmental problems such as electromagnetic interference caused by power systems of earthquake-monitoring stations, navigation systems of unmanned aerial vehicles (UAVs,) and near-Earth space has raised public concerns. Since the 1970s, events have been observed from two pairs of geomagnetically conjugate ground-based stations: Siple station in Antarctica and Roberval station in Quebec and Halley station in Antarctica and St. Anthony station in Newfoundland [2]–[4]. These events have shown that the time-frequency spectrogram of the electric field strength has several parallel horizontal spectral lines separated by 50 Hz/100 Hz or 60 Hz/120 Hz, corresponding to the working frequency of the local terrestrial power system. Similar events have also been observed from satellites including ARIEL-3, OGO-3, AUREOL-3, DEMETER, C/NOFS, and Chibis-M [5]–[10]. They are referred to as power line harmonic radiation (PLHR) and are generally considered as pollutants to the near-Earth space resulting from the power system [11]. PLHR penetration into the lower ionosphere may cause enhanced electron precipitation

The associate editor coordinating the review of this manuscript and approving it for publication was Mohamed Kheir.

and modification of the ionospheric and magnetospheric currents; this radiation can even influence thunderstorm activity [12]–[15].

Nearly coinciding with the discovery of PLHR, magnetospheric line radiation (MLR) was detected by Matthews and Yearby [16]. MLR plays an important role in the space environment because it triggers emissions and influences particles in the radiation belts [17]. It has discrete linear radiations similar to those of PLHR, in which spectral lines have a certain bandwidth accompanied by frequency drift, and the radiation it triggers can sometimes be clearly observed. The interval between spectral lines does not always correspond to the working frequency of the local power system. The typical frequency interval of MLR ranges from 50 Hz to 90 Hz, with a central frequency of 3 kHz and a bandwidth of 1 kHz. Early on, MLR of 3–4 kHz was detected at Halley and St. Anthony stations and by satellites such as ISEE-1 and ISIS, although most cases were not directly related to PLHR [18]–[21]. Manninen reported that MLR occurred most frequently during periods of low geomagnetic activity and in a broad space at low altitudes [22]. These occurrences were believed to be initially triggered by PLHR, but ultimately, their frequency drifted away from the PLHR frequency. According to the DEMETER satellite data, MLR occurs in some cases only when the level of geomagnetic activity is high [23]. These occurrences may be triggered by PLHR radiating from the Earth's surface. When PLHR propagates in the geomagnetic equatorial region, the wave–particle interaction can enhance the wave intensity and change its frequency. Other observations have shown that MLR can be generated naturally, independent of the terrestrial power systems. In addition, the occurrence of PLHR is unlikely related to geomagnetic activities. Its frequency is mainly in the range of 2–3 kHz, whereas MLR is more likely to occur during high geomagnetic activity with a frequency usually below 2 kHz. Further, MLR has a higher intensity than PLHR [24]. Other results indicate that MLR occurs mainly in the plasma layer with the magnetic shell parameter $L > 2$. Its longitudinal span can extend over 100° with a duration of several hours. A slight increase in daytime events has been reported compared with those occurring at night, and events are more common during periods of high geomagnetic activity. In the Northern Hemisphere, more events occur in winter than in summer, whereas MLR events occur mainly in areas with high geomagnetic latitudes that are close to right-hand circular polarization [25]–[29].

Both PLHR and MLR can affect the space environment. However, it remains controversial whether MLR originates from PLHR or whether MLR is irrelevant to PLHR. This study presents a statistical analysis of PLHR and MLR events over China detected by the DEMETER satellite from 2008 to 2010. Section II briefly introduces the DEMETER satellite and the characteristics of its data. In Section III, short-time Fourier transform and Welch power spectrum estimation are used to detect PLHR and MLR events, and the occurrence time, geographical location, and Kp/Dst indices of these events are statistically analyzed and compared. Section IV utilizes singular value decomposition on the magnetic field to analyze the propagation characteristics of MLR in the ionosphere. Section V concludes the study by summarizing the relationship between the two phenomena.

II. DEMETER SATELLITE AND DATA SET

DEMETER, a microsatellite developed by the Centre National d'Etudes Spatiales (French Space Agency), was dedicated to monitoring seismic electromagnetic activities. The satellite's operation time was from June 2004 to December 2010. It traveled in the nearly sun-synchronous polar orbit with an inclination of 98.3°. Its initial orbit height was 710 km, which decreased to 660 km in December 2005. Each satellite orbit was divided into a downward and upward orbit. In the downward orbit, the satellite traveled from north to south and passed through some area at about 10:30 local time. In the upward orbit, the satellite traveled from south to north and passed through some area at about 22:30 local time [30].

DEMETER had two scientific modes: survey and burst. The survey mode was continuously active at geomagnetic latitudes lower than 65° with lower time resolution. The burst mode enabled more detailed data to be collected but was active only above regions of interest, with 80% of the burst-mode data collected over seismic belts. DEMETER measured the electric and magnetic fields using Instrument Champ Electrique (ICE) and Instrument Magnetic Search Coil (IMSC), respectively [31], [32]. In the very low frequency (VLF) range up to 20 kHz, a waveform of one electric field component and one magnetic field component was measured in the burst mode, whereas in the survey mode, their power spectrum was calculated onboard with a predefined frequency resolution of 19.53 Hz. In the extremely low frequency (ELF) range up to 1250 Hz, waveforms of three electric field components and three magnetic field components were measured in the burst mode.

Because the frequency resolution of survey-mode data is insufficient for PLHR and MLR detection, and disturbance from ICE measurement is significantly lower than that from IMSC measurement, we used the VLF- and ELF-range electrical field data in the burst mode to detect PLHR or MLR events in this study. These data cover mainly parts of China with latitude from 75° E to 135° E and longitude from 12° N to 55° N during 2008 to 2010. Notably, DEMETER sent only limited observation data from November 2010 and no data from December 2010 to the ground receiver. Moreover, three magnetic field components in the ELF range were used for wave vector analysis of MLR events.

III. CORRELATION BETWEEN PLHR AND MLR

A. TIME-FREQUENCY ANALYSIS METHOD

This method combines short-time Fourier transform and Welch power spectrum estimation. We obtained the time-frequency power spectrogram of the electric field data in the burst mode by using the following steps, and then we

determined whether they possessed the characteristics of PLHR or MLR.

(1) The electric field strength discrete signal with length N can be expressed as

$$E = E(n) \quad (n = 0, 1, \cdots, N-1) \tag{1}$$

Then, $E(n)$ is divided into a total of M intervals as

$$E(n) = E(m, i)$$
$$(m = 0, 1, \cdots, M-1; i = p, p+1, p+2, \cdots, p+L-1) \tag{2}$$

where L is the length of each interval signal, and each interval has r overlapping points; thus $p = m(L - r)$.

(2) $E(m, i)$ is divided into Q sections as

$$E(m, i) = E_q(m, u)$$
$$(q = 0, 1, \cdots, Q-1; u = h, h+1, \cdots, h+K-1) \tag{3}$$

where each section has K points and s overlapping points; thus $h = p + q(K - s)$. Usually, we take $s = K/2$.

(3) A window function $w(u-h)$ is applied to weight $E_q(m, u)$, and K-point Fourier transform is performed.

$$\bar{E}_q(m, n) = \frac{1}{K} \sum_{u=h}^{h+K-1} w(u-h) E_q(m, u) \mathrm{e}^{2\pi \mathrm{j} n(u-h)/K} \quad (n = 0, 1, \cdots, K/2) \tag{4}$$

(4) The power spectrum of $P(m, n)$ is calculated as

$$P(m, n) = \frac{2K}{f_s W_s Q} \sum_{q=0}^{Q-1} \left| \bar{E}_q(m, n) \right|^2 \tag{5}$$

where f_s is the sampling frequency, W_s is the square root of the window function, $P(m, n)$ is the power spectrum of $E(m, i)$ at frequency $f_n = nf_s/K$, and the corresponding time is $t_m = t_0 + (m + 0.5)(L - r)/f_s$.

(5) All of the power spectra $P(m, n)(m = 0, 1, \cdots, M-1)$ are arrayed according to column sequences, resulting in power spectrum matrix P with dimension of $(K/2 + 1) \times M$. The time corresponding to column n is $(n-1) \times \mathrm{d}t$, and the frequency of row m is $(m\text{-}1) \times \mathrm{d}f$. Here the time resolution is $\mathrm{d}t = L/f_s$, and the frequency resolution is $\mathrm{d}f = f_s/K$.

According to the characteristics of the electrical field waveform data, we took the parameters in the time-frequency analysis as $N = 8192$, $f_s = 40$ kHz, $L = 8192 \times 4$, $r = 0$, $K = 8192$, $Q = 7$, and $s = 4096$. The Hanning window was chosen as the window function: $\mathrm{d}f = 4.8828$ Hz and $\mathrm{d}t = 0.8192$ s.

B. SPECTRUM OF TYPICAL PLHR AND MLR EVENTS

Figure 1 shows the time-frequency power density spectrograms of one typical PLHR event. Ten odd-harmonic spectral lines are clearly visible with frequencies of 50/150/250/1850/1950/2050/2150/2250/2350/2450 Hz, respectively. This feature could be related with the odd harmonics

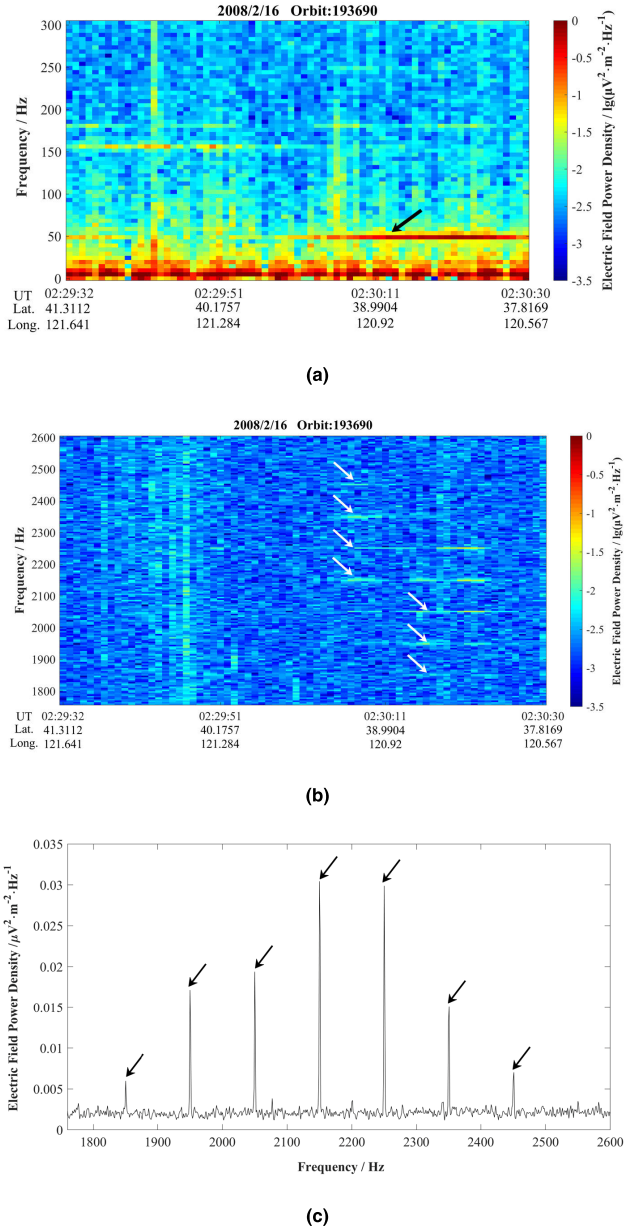

FIGURE 1. (a) 0–300 Hz and (b) 1.8–2.6 kHz time-frequency spectrograms of a typical PLHR event that occurred from 02:30:05 UT to 02:30:27 UT on February 16, 2008, when DEMETER flew over the Circum-Bohai Sea region of China. (c) Large number of odd harmonic spectral lines spaced 100 Hz apart existing in the spectrum (UT: Universal Time; Lat.: Latitude; Long.: Longitude).

caused by wide application of nonlinear devices such as reactors and power electronics in power systems.

The MLR events detected over China were classified into two categories based on their spectral characteristics. The time-frequency spectrograms of typical Class I and Class II events are shown in Figures 2 and 3, respectively. Figure 2(a) shows the time-frequency spectrogram detected by DEMETER when it flew over the Hebei region in China from 13:15:32 Universal Time (UT) to 13:17:00 UT on September 22, 2010. This event shows multiple parallel-strip

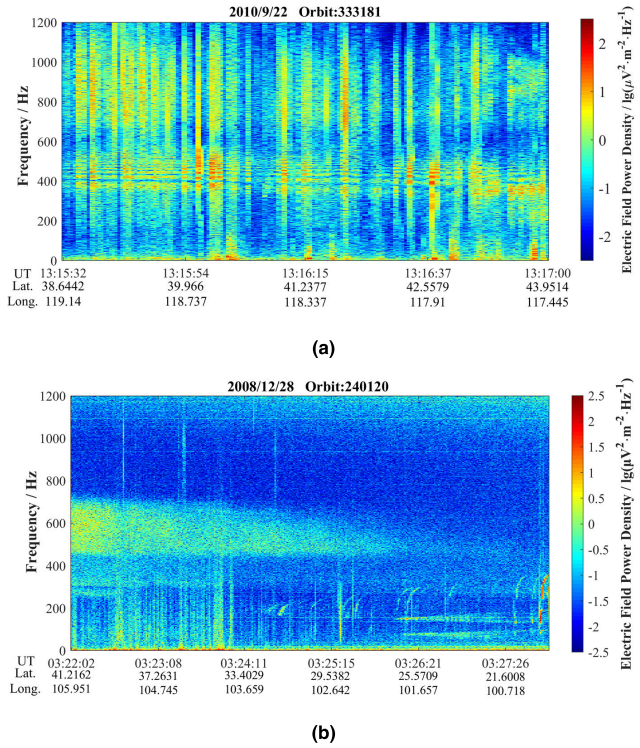

FIGURE 2. Time-frequency spectrograms of typical Class I-MLR event. (a) Event occurring between 13:15:32 UT and 13:17:00 UT on September 22, 2010, when the satellite flew over the Hebei region in China. (b) Event occurring between 03:22:02 UT and 03:27:58 UT on December 28, 2008, when the satellite flew over the Sichuan and Yunnan regions in China.

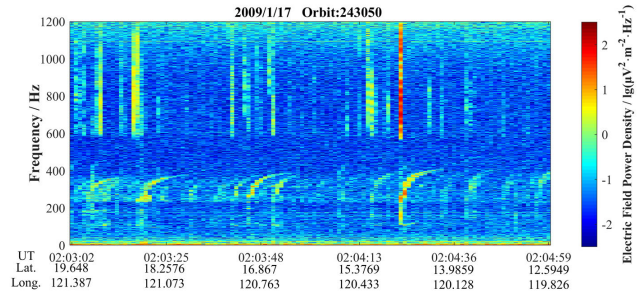

FIGURE 3. Time-frequency spectrogram of typical Class II-MLR event occurring between 02:03:02 UT and 02:04:59 UT on January 17, 2009, when the satellite flew over the South China Sea and the surrounding regions.

spectral lines with frequency drift between 300 Hz and 600 Hz with no triggered radiations. The line bandwidth gradually decreases with increases in frequency. The frequency interval between spectral lines was about 35 Hz; the frequency drift was about 24 Hz; and the frequency drifting speed is about 0.39 Hz/s. Figure 2(b) shows a time-frequency spectrogram detected by DEMETER when it flew over China's Sichuan and Yunnan regions from 03:22:02 UT to 03:27:58 UT on December 28, 2008. Two parallel-strip spectral lines are clearly visible below 200 Hz. Their central frequencies are about 74 Hz and 152 Hz, with a frequency interval of about 78 Hz, frequency drift of about 22 Hz, and frequency drifting speed of about 0.28 Hz/s. Unlike that in Figure 2(a), the parallel spectral lines in Figure 2(b) indicate that rising-tone radiation was triggered, which began at 165 Hz and ended at 357 Hz. The period of these triggered radiations was approximately 4 s, corresponding to the whistle wave duration transmitting from one hemisphere through the magnetosphere to the magnetic conjugate point in the other hemisphere and then reflecting to the original position [16]. A total of 135 events of Class I were detected, 94 of which included triggered radiation. The frequency drifting speed of the parallel spectral lines was between 0 Hz/s and 1 Hz/s, with 94% of events having a frequency drifting speed between 0 Hz/s and 0.4 Hz/s.

The time-frequency spectrogram of the Class II event showed only the triggered radiation with no parallel spectral lines as the baseline. Figure 3 shows a time-frequency spectrogram detected by the satellite flying over the South China Sea and the surrounding regions between 02:03:02 UT and 02:04:59 UT on January 17, 2009. A cluster of rising hook-shaped radiation events can be distinguished between 100 Hz and 500 Hz. Their triggered starting point was approximately 120 Hz, and the ending point was approximately 410 Hz. Unlike that of Class I events, the triggered radiation of Class II events does not have significant baseline support, i.e., parallel spectral lines cannot be found. This is possibly because the baseline radiation is attenuated during transmission and is thus undetectable by the satellite, whereas the triggered radiation is sufficiently strong for detection. A total of 193 events of Class II have been detected.

C. STATISTICAL RESULTS AND DISCUSSIONS

Among the 4228 semi-orbit data files collected from 2008 to 2010, 114 PLHR events and 328 MLR events including 135 cases of Class I events and 193 cases of Class II events were detected. The statistical analysis of time including the year, season, and day or night status; geographical location; and Kp/Dst index distribution for these events are presented below.

1) TEMPORAL DISTRIBUTION

Table 1 shows the annual and monthly distributions of the detected PLHR and MLR events over China during 2008 to 2010. Notably, one-third of the data in November and all data in December 2010 were missing. Therefore, fewer MLR and PLHR events appear to have occurred in 2010 than in 2009. The table shows an annually increasing trend in the number of PLHR and MLR events. However, 57 and 42 PLHR events occurred in 2009 and 2010, respectively, which is significantly higher than the 12 events occurring in 2008. During the same years, 128 and 97 MLR events occurred, respectively, which is similar in number to the 103 MLR events recorded in 2008. From 2008 to 2010, the electrical power generation and consumption in China increased annually at 7.2% and 6.4%, respectively, from 2008 to 2009 and 13.4% and 14.7%, respectively,

TABLE 1. Annual and monthly distributions of PLHR and MLR events over china.

Year/Month		Jan.	Feb.	Mar.	Apr.	May	Jun.	Jul.	Aug.	Sep.	Oct.	Nov.	Dec.	Sum
2008	PLHR	1	3	0	0	0	0	0	0	1	0	1	6	12
	MLR	11	6	4	9	10	7	7	5	5	7	13	19	103
2009	PLHR	2	9	4	1	2	0	2	0	2	13	12	10	57
	MLR	15	4	3	13	9	10	14	3	5	16	16	20	128
2010	PLHR	6	6	9	1	0	1	2	1	2	8	9	-	45
	MLR	12	11	7	5	9	10	9	10	6	9	9	-	97
Sum	PLHR	9	18	13	2	2	1	4	1	5	21	22	16	114
	MLR	38	21	14	27	28	27	30	18	16	32	38	39	328

from 2009 to 2010 [33]–[35]. In particular, the Jindongnan–Nanyang–Jingmen UHV 1000 kV AC transmission line was put into operation in January 2009, followed by the Xiangjiaba–Shanghai UHV ± 800 kV DC transmission line in July 2009. Their operation marked a new era in China's UHV power system development. The rapid increase in PLHR events in 2009 appears to be related to the development of the Chinese power system, although no obvious connection has been made between the power system and the number of MLR events.

China is located in the Northern Hemisphere between 4° N and 53° N. Because most of mainland China is a temperate region, the seasons are divided by changes in solar radiation, including spring from March to May, summer from June to August, autumn from September to November, and winter from December to February. 43.9% of MLR events occur in spring and summer, whereas 56.1% occur in autumn and winter. 19.3% of PLHR events occur in spring and summer, whereas 81.7% occur in autumn and winter. The seasonal variation for MLR is less than that for PLHR, with slightly more events occurring in autumn and winter. The seasonal difference in PLHR/MLR can be attributed to the seasonal variation in electron density, which is an important ionospheric parameter. The electron density in summer tends to be higher than that in winter, causing electromagnetic radiation such as PLHR and MLR to be more seriously attenuated and harder to detect. 86.0% of MLR events occur during the daytime. The number of daytime PLHR events accounts for 93.7% of the total. Therefore, both MLR and PLHR show significant diurnal differences.

2) GEOGRAPHICAL DISTRIBUTION

We compared the locations of PLHR and MLR event occurrences. Because the spectrogram of Class II MLR events triggered only radiation and no baseline, the occurrence locations could not be determined. Therefore, we analyzed only the locations of Class I MLR events. Figure 4 shows the geographical distribution of 114 PLHR events and 135 MLR events. The PLHR events are marked by blue lines in the figure, whereas the center points of the baselines of MLR events are marked by red triangles. The PLHR events were distributed mostly in the range of 20° N–45° N; however, the MLR events were distributed near the southwestern border, at 18° N–28° N. Few Class I MLR events occurred in the middle- to high-latitude region at 35°N and higher, which differs from the findings of Němec's such that MLR events occur mainly in middle- and high-latitude regions [24]. On the basis of their geographical distribution, the two phenomena appear to be unrelated.

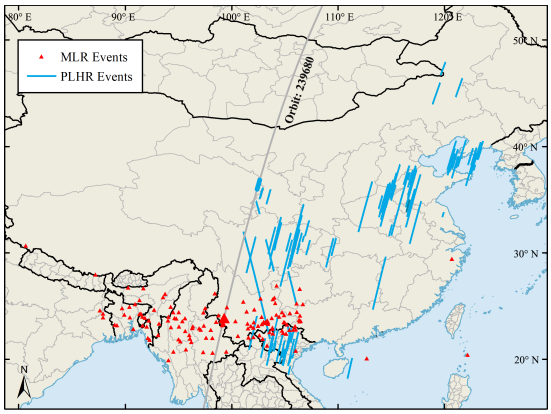

FIGURE 4. Geographical distribution of PLHR events (blue lines) and MLR events (red triangles). The MLR and PLHR events in orbit 239680 (gray line) occurred at different locations.

Additionally, among the 328 MLR events, only 24 MLR events occurred in the same orbit as PLHR, e.g., orbit 239680 shown in Figure 4. However, PLHR and MLR events were distributed at different locations and showed negligible correlation.

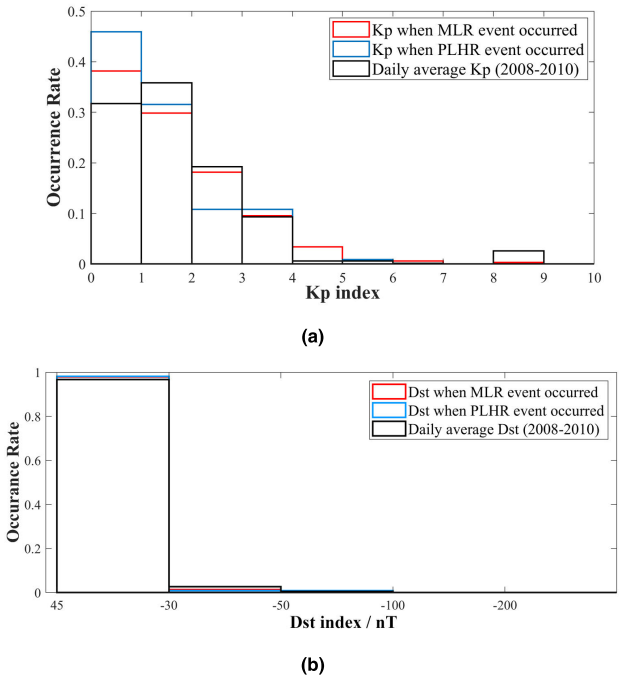

FIGURE 5. Comparison of (a) Kp and (b) Dst indices distribution of PLHR and MLR events that occurred during the daytime. The blue (red) line represents the indices at the occurrence time of PLHR (MLR) events. The daily average Kp and Dst indices in the three years from 2008 to 2010 are represented by black lines.

3) KP AND DST INDICES

We used the Kp and Dst indices from National Aeronautics and Space Administration (NASA) Goddard Space Flight Center (https://cdaweb.sci.gsfc.nasa.gov/index.html/) to characterize the geomagnetic disturbance. The Kp index reflects the global geomagnetic activity level. When $0 \leq \text{Kp} < 2$, the geomagnetic field is calm; when $\text{Kp} \geq 5$, the geomagnetic activity level is considered to be a geomagnetic storm. The Dst index is the geomagnetic index monitored hourly at stations in middle and low latitudes. A lower Dst value reflects a more intense geomagnetic activity level. A value of $-50\ \text{nT} < \text{Dst} \leq -30\ \text{nT}$ indicates a small magnetic storm; $-100\ \text{nT} < \text{Dst} \leq -50\ \text{nT}$ indicates a medium-sized magnetic storm, $-200\ \text{nT} < \text{Dst} \leq -100\ \text{nT}$ indicates a large magnetic storm, and $\text{Dst} \leq -200\ \text{nT}$ signifies a very large magnetic storm. To avoid diurnal differences in the ionospheric state and, in particular, the effects of changes in electron density, we analyzed only 93.7% of PLHR events and 86% of MLR events that occurred during daytime, for totals of 106 and 282 events, respectively. Figure 5 shows the distributions of the Kp and Dst indices and their daily averages at the occurrence time of these events. The daily average was calculated on the basis of the distribution of all Kp and Dst indices from 2008 to 2010.

As shown in Figure 5a, among the daily average Kp distributions, the proportion of $\text{Kp} < 2$ was 67.5%, and that of $\text{Kp} > 5$ was 3.3%. 77.5% of PLHR events occurred at $\text{Kp} < 2$, and 0.9% of PLHR events occurred at $\text{Kp} > 5$. However, 68.0% of MLR events occurred at$\text{Kp} < 2$, and 0.9% of MLR events occurred at $\text{Kp} > 5$. It can be concluded that Kp index distributions are consistent with the daily distribution trends at the times of PLHR and MLR event occurrences, and no obvious preference is indicated. Figure 5b shows that $\text{Dst} > -30$ nT accounted for 96.7% among the daily average distributions. 98.2% of PLHR events occurred at $\text{Dst} > -30$ nT, whereas 97.9% of MLR events occurred at $\text{Dst} > -30$ nT. It is therefore apparent that when PHR and MLR events occurred, the Dst index distributions remained consistent with their daily distribution trends and showed no obvious preference. It can be concluded that neither PLHR nor MLR are significantly correlated with the geomagnetic activity level.

IV. PROPAGATION CHARACTERISTICS ANALYSIS

It is believed that PLHR propagates along the geomagnetic field in a whistling mode in the ionosphere according to right-handed circular polarization [36]–[38]. This study used the Magnetic Singular Value Decomposition Method [39] to analyze the propagation characteristic of MLR in the ionosphere. The details are described below.

Three components of the magnetic field in the original satellite coordinate system were transformed into a local geomagnetic coordinate (LGM) system where the origin is the center of the satellite; the Z-axis indicates the direction of the geomagnetic field determined by the 12th generation of the International Geomagnetic Reference Field model (IGRF-12); the Y-axis is perpendicular to the plane defined by the Z-axis and the line connecting the Earth's center to the satellite; and the X axis is determined by the right-hand rule based on the Y- and Z-axes. We assume that the three components of the magnetic field in LGM are

$$\boldsymbol{B} = B_1\bar{x} + B_2\bar{y} + B_3\bar{z} \tag{6}$$

where $B_i (i = 1, 2, 3)$ is the component of $\boldsymbol{B}$ along different axis. It is assigned such that

$$S_{ij} = B_i B_j^* (i, j = 1, 2, 3) \tag{7}$$

where S_{ij} is the spectrum matrix of the magnetic field, and $*$ represents the conjugate of B_j. The following real matrix $\mathbf{A}$ with dimensions of 6×3 was constructed by using the real and imaginary parts of S_{ij}.

$$A = \begin{pmatrix} \text{Re}(S_{11}) & \text{Re}(S_{12}) & \text{Re}(S_{13}) \\ \text{Re}(S_{12}) & \text{Re}(S_{22}) & \text{Re}(S_{23}) \\ \text{Re}(S_{13}) & \text{Re}(S_{23}) & \text{Re}(S_{33}) \\ 0 & -\text{Im}(S_{12}) & -\text{Im}(S_{13}) \\ \text{Im}(S_{12}) & 0 & -\text{Im}(S_{23}) \\ \text{Im}(S_{13}) & \text{Im}(S_{23}) & 0 \end{pmatrix} \tag{8}$$

Singular value decomposition was performed on matrix $\mathbf{A}$ to derive

$$\mathbf{A} = \mathbf{U}\mathbf{W}\mathbf{V}^{\mathrm{T}} \tag{9}$$

where $\mathbf{U}$ is a 6×3 dimensional matrix consisting of standard orthogonal column vectors, $\mathbf{W}$ is a diagonal array of three

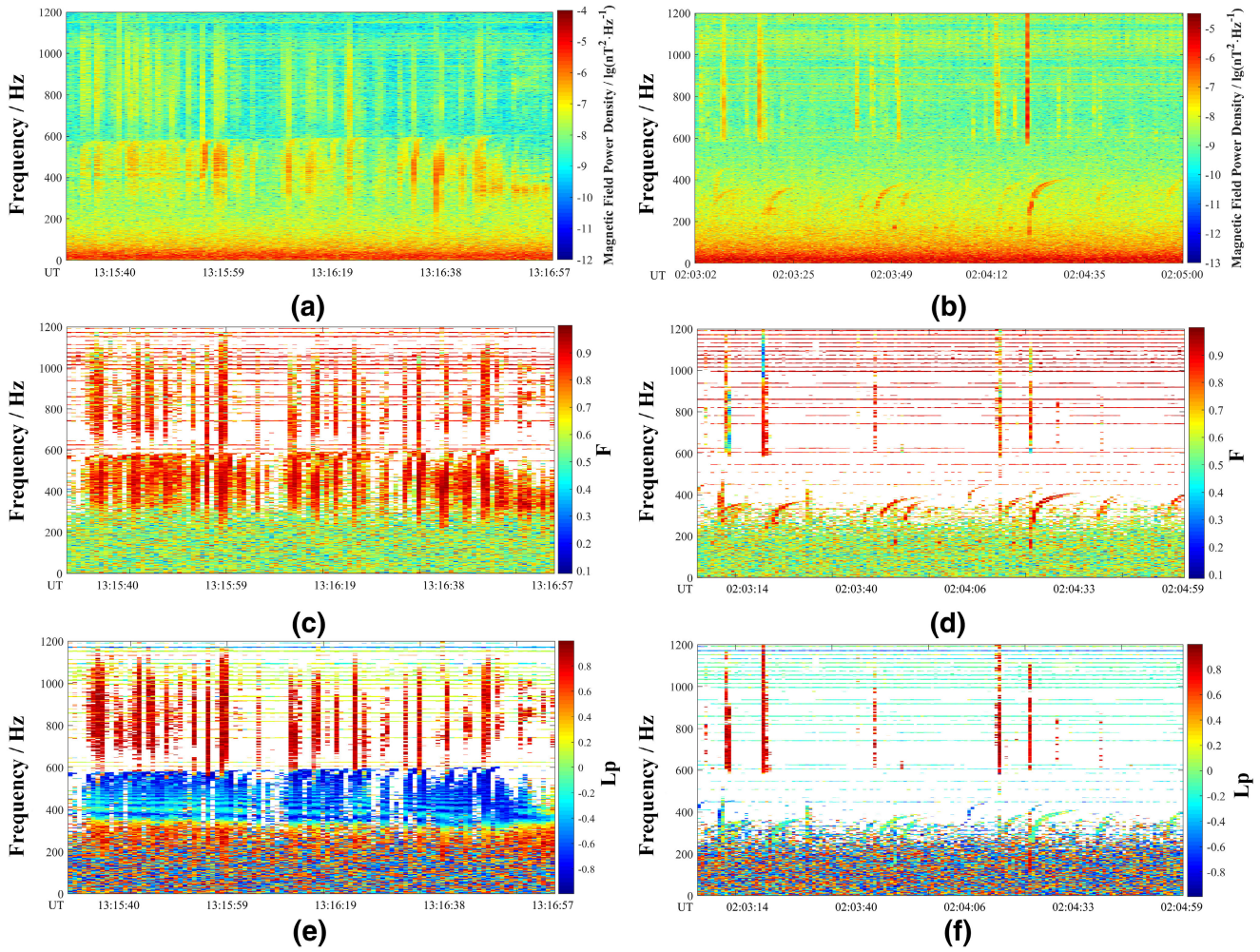

FIGURE 6. Wave vector characteristics of typical Class I and Class II MLR events. (a) Time-frequency spectrum of magnetic field for Class I event. (b) Time-frequency spectrum of magnetic field for Class II event. (c) Planarity for Class I event. (d) Planarity for Class II event. (e) Ellipticity for Class I event. (f) Ellipticity for Class II event.

non-negative eigenvalues, and $\mathbf{V}^{\mathrm{T}}$ is a 3 × 3 dimensional matrix consisting of standard orthogonal row vectors. By arranging the three eigenvalues in $\mathbf{W}$ from small to large, we get w_1, w_2, and w_3. The least square estimator of the wave vector is the eigenvector row vector $\boldsymbol{k}^*$ of $\mathbf{V}^{\mathrm{T}}$ corresponding to w_1. The other two eigenvector row vectors of $\mathbf{V}^{\mathrm{T}}$ make up the polarization plane of the magnetic field, where the row vector corresponding to w_2 is the direction of the polarization short axis and that corresponding to w_3 is the direction of the polarization long axis. We define the magnetic field polarization planarity function F as

$$F = 1 - \sqrt{w_1/w_3} \tag{10}$$

A value of $F \rightarrow 1$ indicates high planarity of the wave. That of $F < 1$, particularly when its value is very low, indicates that the noise interference to the wave is high, the planarity is low, or there is no wave of a certain frequency. The polarization ellipticity and rotation direction function L_p is defined as

$$L_p = \mathrm{sign}[\mathrm{Im}(S_{12})] \cdot (w_2/w_3) \tag{11}$$

where sign(·) is a symbolic function. If $L_p \rightarrow 1$, the wave features right-handed circular polarization; if $L_p \rightarrow$ -1, the wave features left-handed circular polarization; if $L_p \rightarrow 0$, the wave is linear polarized.

By using the wave vector analysis method, we analyzed the three components of the magnetic field at the ELF-frequency band to obtain the planarity and ellipticity of MLR waves. Figure 6 shows results of wave vector analysis of typical Class I-MLR (Figure 2(a)) and Class II-MLR events (Figure 3). Figures 6(a) and (b) characterize the time-frequency spectrograms of the magnetic fields. Figure 6(a) shows the same parallel-strip drifting spectral lines between 300 Hz and 600 Hz as those shown in Figure 2(a), and the cluster of radiation events shown in Figure 3 occur between 100 Hz and 500 Hz in Figure 6(b). Figures 6(c) and (d) characterize the polarization planarity (F) of the waves. The values of F,

in which the MLR occurrences are close to 1, shows that MLR has higher planarity. Figures 6(e) and (f) characterize the ellipticity (L_p) of the wave. It is apparent that the values of L_p, in which the MLR occurrences are approximately zero, implies that MLR is close to linear polarization. On the basis of the above analysis, MLR over China can be considered as a wave propagating in linear polarization.

The propagation characteristics of MLR detected in the areas of low to middle latitude are different from those reported in previous research [29] owing possibly to differences in the geomagnetic latitude. The polarization mode of MLR is different from that of PLHR. This does not exclude the possibility of MLR being triggered by PLHR. However, the triggered radiation of PLHR detected thus far occurred in high-latitude areas [40], [41]. The MLR detected over China could not have propagated from high to low latitudes because of its wave vector characteristics. It is therefore impossible for MLR over China to be triggered by PLHR.

V. CONCLUSION

In this study, we systematically analyzed PLHR and MLR events observed by DEMETER as it flew over China from 2008 to 2010. By using short-time Fourier transform and Welch power spectrum estimation, 114 PLHR events and 328 MLR events were identified from 4228 data files in the burst mode. We studied the correlations between PLHR and MLR based on the occurrence time, geographical distribution, Kp and Dst indices, and propagation characteristics. The main findings are summarized in the following points.

(1) Regarding the occurrence time, the numbers of PLHR and MLR events increased yearly, although the number of PLHR events increased more rapidly. This result is closely related to the development of a terrestrial power system. In addition, PLHR was discovered to be influenced by the structure of the power system. The MLR growth was relatively stable and did not appear to be correlated with the power system or other human activities. Both types of events showed diurnal and seasonal differences. The events occurred more often during the daytime and in autumn or winter. The ionospheric state, i.e., the electron density, also showed seasonal differences, indicating that PLHR and MLR events have similar occurrence conditions and are related to the ionospheric state.

(2) PLHR was distributed mostly in the region of 20° N–45° N over China with a high population density and intensive social and economic activity. MLR was concentrated in southwestern low-latitude regions at 18°N–28°N. No correlation was found concerning the distribution location for the two types of events.

(3) Neither the PLHR nor MLR events showed preference based on the Kp or the Dst indices. Moreover, their occurrences were not significantly correlated with the geomagnetic activity level.

(4) PLHR wave is believed to propagate along the Earth's magnetic field in a right-handed circular polarization. The propagation of MLR wave, however, is linearly polarized over the mid-latitude regions, according to the singular value decomposition-based method.

On the basis of these findings, we conclude that the MLR phenomenon over China is not directly correlated with the PLHR phenomenon. PLHR and MLR have some similarities: They are both related to the ionospheric state and are weakly influenced by geomagnetic activities. However, differences are apparent in their occurrence time and location as well as their propagation mode in the ionosphere, which indicates that sources of these two radiation types are different. MLR is more likely radiation generated by natural factors, whereas PLHR is closely related to radiation from terrestrial power systems. Because both phenomena can trigger other radiation events in the ionosphere and have the potential to pollute the near-earth space environment, their formation mechanisms should be studied further.

ACKNOWLEDGMENT

The authors gratefully acknowledge Centre de Données de la Physique des Plasmas (CDPP) (https://cdpp-archive.cnes.fr/) to provide the observation data of DEMETER.

REFERENCES

[1] Y. Li, S. Yuan, W. Liu, G. Zhang, Y. Teng, and X. Chen, "A fast method for reliability evaluation of ultra high voltage AC/DC system based on hybrid simulation," *IEEE Access*, vol. 6, pp. 19151–19160, 2018.
[2] R. A. Helliwell, J. P. Katsufrakis, T. F. Bell, and R. Raghuram, "VLF line radiation in the earth's magnetosphere and its association with power system radiation," *J. Geophys. Res.*, vol. 80, no. 31, pp. 4249–4258, Nov. 1975.
[3] C. G. Park and R. A. Helliwell, "Power line radiation in the magnetosphere," *Adv. Space Res.*, vol. 1, no. 2, pp. 423–437, 1981.
[4] K. H. Yearby, A. J. Smith, T. R. Kaiser, and K. Bullough, "Power line harmonic radiation in newfoundland," *J. Atmos. Terr. Phys.*, vol. 45, no. 6, pp. 409–419, Jun. 1983.
[5] J. P. Luette, C. G. Park, and R. A. Helliwell, "The control of the magnetosphere by power line radiation," *J. Geophys. Res.*, vol. 84, no. A6, pp. 2657–2660, Jun. 1979.
[6] K. Bullough, "Satellite observations of power line harmonic radiation," *Space Sci. Rev.*, vol. 35, no. 2, pp. 175–183, Jun. 1983.
[7] M. Parrot, "Observations of power line harmonic radiation by the low-altitude AUREOL 3 satellite," *J. Geophys. Res.*, vol. 99, no. A3, pp. 3961–3969, Mar. 1994.
[8] F. Dudkin, V. Korepanov, D. Dudkin, V. Pilipenko, V. Pronenko, and S. Klimov, "Electric field of the power terrestrial sources observed by microsatellite chibis-M in the earth's ionosphere in frequency range 1–60 Hz," *Geophys. Res. Lett.*, vol. 42, no. 14, pp. 5686–5693, Jul. 2015.
[9] R. Pfaff, H. Freudenreich, F. Simoes, and C. Liebrecht, "Observations of 50/60 Hz power line radiation in the low latitude ionosphere detected by the electric field instrument on the C/NOFS satellite," in *Proc. 31st URSI Gen. Assem. Sci. Symp. (URSI GASS)*, Beijing, China, vol. 2014, p. 1.
[10] J. Wu, C. Zhang, L. Zeng, and Q. Ma, "Systematic investigation of power line harmonic radiation in near-Earth space above China based on observed satellite data," *J. Geophys. Res., Space Phys.*, vol. 122, no. 3, pp. 3448–3458, Mar. 2017.
[11] K. Bullough, "Power line harmonic radiation: Sources and environmental effects," in *Handbook of Atmospheric Electrodynamics*, vol. 2. Boca Raton, FL, USA: CRC Press, 1995, pp. 292–328.
[12] K. Bullough, A. R. L. Tatnall, and M. Denby, "Man-made e.l.f./v.l.f. emissions and the radiation belts," *Nature*, vol. 260, no. 5550, pp. 401–403, Apr. 1976.
[13] O. Molchanov and M. Parrot, "PLHR emissions observed on satellites," *J. Atmos. Terr. Phys.*, vol. 57, no. 5, pp. 493–505, Apr. 1995.
[14] Y. Ando, M. Hayakawa, and O. A. Molchanov, "Theoretical analysis on the penetration of power line harmonic radiation into the ionosphere," *Radio Sci.*, vol. 37, no. 6, pp. 1–12, Dec. 2002.

[15] J. Wu, Q. Guo, X. Yan, and C. Zhang, "Theoretical analysis on affecting factors of power line harmonic radiation," *IEEE Trans. Plasma Sci.*, vol. 47, no. 1, pp. 770–775, Jan. 2019.

[16] J. P. Matthews and K. Yearby, "Magnetospheric VLF line radiation observed at Halley, Antarctica," *Planet. Space Sci.*, vol. 29, no. 1, pp. 97–106, Jan. 1981.

[17] M. Parrot and F. Němec, "MLR events and associated triggered emissions observed by DEMETER," *Adv. Space Res.*, vol. 44, no. 9, pp. 979–986, Nov. 2009.

[18] K. H. Yearby, "Magnetospheric VLF line radiation," Ph.D. dissertation, Dept. Phys., Sheffield Univ., Sheffield, U.K., 1982.

[19] T. F. Bell, J. P. Luette, and U. S. Inan, "ISEE 1 observations of VLF line radiation in the earth's magnetosphere," *J. Geophys. Res., Space Phys.*, vol. 87, no. A5, pp. 3530–3536, May 1982.

[20] H. C. Koons, "Whistlers and whistler-stimulated emissions in the outer magnetosphere," *J. Geophys. Res.*, vol. 90, no. A9, pp. 8547–8551, Sep. 1985.

[21] C. J. Rodger, "Is magnetospheric line radiation man-made?" *J. Geophys. Res.*, vol. 105, no. A7, pp. 15981–15990, Jul. 2000.

[22] J. Manninen, "Some aspects of ELF-VLF emissions in geophysical research," Ph.D. dissertation, Dept. Sci., Oulu Univ., Oulu, Finland, 2005.

[23] M. Parrot, J. Manninen, O. Santolík, F. Nemec, T. Turunen, T. Raita, and E. Macúšová, "Simultaneous observation on board a satellite and on the ground of large-scale magnetospheric line radiation," *Geophys. Res. Lett.*, vol. 34, no. 19, Oct. 2007, Art. no. L19102.

[24] F. Němec, O. Santolík, M. Parrot, and J. J. Berthelier, "Comparison of magnetospheric line radiation and power line harmonic radiation: A systematic survey using the DEMETER spacecraft," *J. Geophys. Res.*, vol. 112, no. A4, Apr. 2007, Art. no. A04301.

[25] F. Němec, M. Parrot, O. Santolík, C. J. Rodger, M. J. Rycroft, M. Hayosh, D. Shklyar, and A. Demekhov, "Survey of magnetospheric line radiation events observed by the DEMETER spacecraft," *J. Geophys. Res.*, vol. 114, no. A5, May 2009, Art. no. A05203.

[26] F. Němec, "Conjugate observations on board a satellite and on the ground of a remarkable MLR-like event," *Geophys. Res. Lett.*, vol. 36, no. L22, Nov. 2009, Art. no. L22103.

[27] F. Němec, M. Parrot, and O. Santolík, "Detailed properties of magnetospheric line radiation events observed by the DEMETER spacecraft," *J. Geophys. Res.*, vol. 117, no. A5, May 2012, Art. no. A05210.

[28] F. Němec, "Magnetospheric line radiation event observed simultaneously on board cluster 1, cluster 2 and DEMETER spacecraft," *Geophys. Res. Lett.*, vol. 39, no. L18, Sep. 2012, Art. no. L18103.

[29] B. Bezděková, F. Nemec M. Parrot, O. Santolík, and O. Kruparova, "Magnetospheric line radiation: 6.5 years of observations by the DEMETER spacecraft," *J. Geophys. Res., Space Phys.*, vol. 120, no. 11, pp. 9442–9456, Nov. 2015.

[30] D. Lagoutte, "DEMETER microsatellite scientific mission center data product description," DEMETER Sci. Mission Center, Orléans, France, Tech. Rep. DMT-SP-9-CM-6054-LPC, Jun. 2006.

[31] J. J. Berthelier, M. Godefroy, F. Leblanc, M. Malingre, M. Menvielle, D. Lagoutte, J. Y. Brochot, F. Colin, F. Elie, C. Legendre, P. Zamora, D. Benoist, Y. Chapuis, J. Artru, and R. Pfaff, "ICE, the electric field experiment on DEMETER," *Planet. Space Sci.*, vol. 54, no. 5, pp. 456–471, Apr. 2006.

[32] M. Parrot, D. Benoist, J. J. Berthelier, J. Błęcki, Y. Chapuis, F. Colin, F. Elie, P. Fergeau, D. Lagoutte, F. Lefeuvre, C. Legendre, M. Lévêque, J. L. Pinçon, B. Poirier, H.-C. Seran, and P. Zamora, "The magnetic field experiment IMSC and its data processing onboard DEMETER: Scientific objectives, description and first results," *Planet. Space Sci.*, vol. 54, no. 5, pp. 441–455, Apr. 2006.

[33] *China Electric Power Yearbook Editorial Board, China Electric Power Yearbook-2008*, China Electricity Press, Beijing, China, 2008.

[34] *China Electric Power Yearbook Editorial Board, China Electric Power Yearbook-2009*, China Electricity Press, Beijing, China, 2009.

[35] *China Electric Power Yearbook Editorial Board, China Electric Power Yearbook-2010*, China Electricity Press, Beijing, China, 2010.

[36] C. Capetanopoulos and R. B. Kieburtz, "Excitation of the whistler mode in the ionosphere by leakage from VLF guided-wave modes," *Radio Sci.*, vol. 1, no. 8, pp. 859–875, Aug. 1966.

[37] F. Němec, "Power line harmonic radiation observed by the DEMETER spacecraft at 50/60 Hz and low harmonics," *J. Geophys. Res.*, vol. 111, no. 10, Apr. 2006, Art. no. A04308.

[38] F. Němec, "Power line harmonic radiation observed by satellite: Properties and propagation through the ionosphere," *J. Geophys. Res.*, vol. 113, no. A8, Aug. 2008, Art. no. A08317.

[39] O. Santolík, M. Parrot, and F. Lefeuvre, "Singular value decomposition methods for wave propagation analysis," *Radio Sci.*, vol. 38, no. 1, p. 1010, Feb. 2003.

[40] F. Němec, M. Parrot, and O. Santolík, "Influence of power line harmonic radiation on the VLF wave activity in the upper ionosphere: Is it capable to trigger new emissions?" *J. Geophys. Res.*, vol. 115, no. A11, Nov. 2010, Art. no. A11301.

[41] M. Parrot, F. Němec, and O. Santolík, "Statistical analysis of VLF radio emissions triggered by power line harmonic radiation and observed by the low-altitude satellite DEMETER," *J. Geophys. Res., Space Phys.*, vol. 119, no. 7, pp. 5744–5754, Jul. 2014.

QIANG GUO (M'19) was born in Yangzhou, Jiangsu, China, in 1995. He received the B.S. degree in electrical engineering and automation from Beihang University, Beijing, China, in 2017, where he is currently pursuing the M.S. degree in electrical engineering. His current research interests include electromagnetic environment of the power grid and electromagnetic measurement technology.

JING WU (M'18) was born in Suzhou, Anhui, China, in 1978. She received the Ph.D. degree in electrical engineering from Tsinghua University, Beijing, China, in 2006. Since 2012, she has been an Associate Professor with the School of Automatic Science and Electrical Engineering, Beihang University. From 2017 to 2018, she was a Visiting Scholar with the Department of Atmosphere and Ocean System, University of California at Los Angeles, Los Angeles, CA, USA. Her current research interests include the electromagnetic environment of high-voltage transmission lines, electromagnetic nondestructing testing, and the design on precise electrical apparatus.

CHAO YUE was born in Hubei, China. She received the Ph.D. degree from the Department of Atmospheric and Oceanic Sciences, University of California at Los Angeles, Los Angles (UCLA), LA, CA, USA, in 2015, where she has been an Assistant Researcher, since 2017. Her current research interests include investigating EMIC wave in the inner magnetosphere, and the ring current features and the relative contributions from different species with different energies.

LI XIE was born in Xinjiang, China, in 1980. She received the Ph.D. degree in electrical engineering from Beihang University, Beijing, China, in 2010. She has been an Engineer with the Electric Power Research Institute of China, since 2010. Her main research interest includes electromagnetic environment of high-voltage transmission lines.